Large Single Crystals of Two-Dimensional π-Conjugated Metal–Organic Frameworks via Biphasic Solution-Solid Growth

Dong-Gwang Ha, Mehdi Rezaee, Yimo Han, Saima A. Siddiqui, Robert W. Day, Lilia S. Xie, Brian J. Modtland, David A. Muller, Jing Kong, Philip Kim, Mircea Dincă,* and Marc A. Baldo*

Cite This: https://dx.doi.org/10.1021/acscentsci.0c01488

Read Online

ACCESS | Metrics & More | Article Recommendations | Supporting Information

ABSTRACT: Two-dimensional (2D) π-conjugated metal–organic frameworks (πMOFs) are a new class of designer electronic materials that are porous and tunable through the constituent organic molecules and choice of metal ions. Unlike typical MOFs, 2D πMOFs exhibit high conductivity mediated by delocalized π-electrons and have promising applications in a range of electrical devices as well as exotic physical properties. Here, we develop a growth method that generates single-crystal plates with lateral dimensions exceeding 10 μm, orders of magnitude bigger than previous methods. Synthesis of large single crystals eliminates a significant impediment to the fundamental characterization of the materials, allowing determination of the intrinsic conductivity and mobility along the 2D plane of πMOFs. A representative 2D πMOF, Ni-CAT-1, exhibits a conductivity of up to 2 S/cm, and Hall measurement reveals the origin of the high conductivity. Characterization of crystalline 2D πMOFs creates the foundation for developing electronic applications of this promising and highly diverse class of materials.
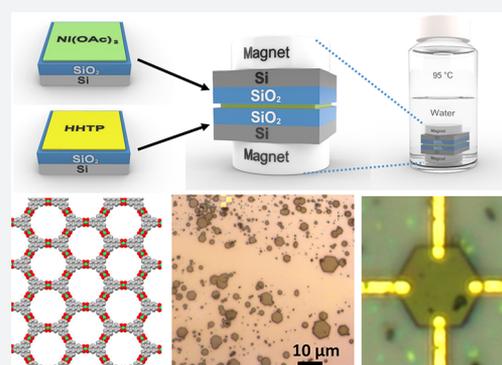
INTRODUCTION

Metal–organic frameworks (MOFs) are porous materials with a customizable crystalline structure that can be designed from building blocks of organic molecules and metal ions.[1−3] They are typically insulators, but two-dimensional (2D) π-conjugated MOFs (πMOFs) can exhibit high electrical conductivity, making them good candidates for a range of electrical devices.[4−6] Similar to other 2D electronic materials such as graphene, 2D πMOFs exhibit π-conjugation in the basal plane, with neighboring layers associated more loosely through van der Waals forces along the c axis. Numerous theoretical calculations have suggested that some of these 2D πMOFs should exhibit exotic electronic properties arising from topologically nontrivial band structures.[7−9] This potentially new physics has sparked additional interest in this novel class of electronic materials and has inspired the synthesis of various 2D πMOFs.[10,11] Nevertheless, a major bottleneck toward exploring such properties has been crystal growth, especially within the basal plane where intrinsic high conductivity is expected. Because of limitations in the available crystal size of 2D πMOFs, conventional electrical characterization including a Hall effect measurement of the basal plane has been technically challenging. The typical basal plane domain size afforded by conventional crystal growth techniques has thus far been limited to less than 200 nm,[5,12−17] which is challenging for multiterminal device fabrication especially given the needle-like morphology. As such, one of the key challenges preventing a deeper understanding of the electronic properties of these materials has been the growth of sufficiently large single crystals.

Two methods are commonly used to synthesize 2D πMOFs for electrical characterization: single-phase solution synthesis and liquid–liquid interfacial synthesis. The former typically consists of homogeneous reactions carried out by dissolving and heating the constituent organic ligands and metal salts in a solvent. The primary crystal growth direction is usually the c axis, yielding needle-shaped crystals with very small cross sections in the basal plane.[12−15] It has proven exceedingly difficult to increase the basal plane crystal cross-section through single-phase solution growth. We hypothesize that the large reaction volume reduces the collision probability of reactants and crystal nuclei. The reaction is further impeded as the small nuclei precipitate and become covered by other nuclei. Conversely, the challenge for the liquid–liquid interfacial method is that the reaction occurs at the boundary of immiscible solutions. Unlike in the single-phase method, liquid–liquid interfacial reactions are performed at room temperature,[17−22] or with marginal heating.[23] Because the reaction temperature is a key parameter governing crystal
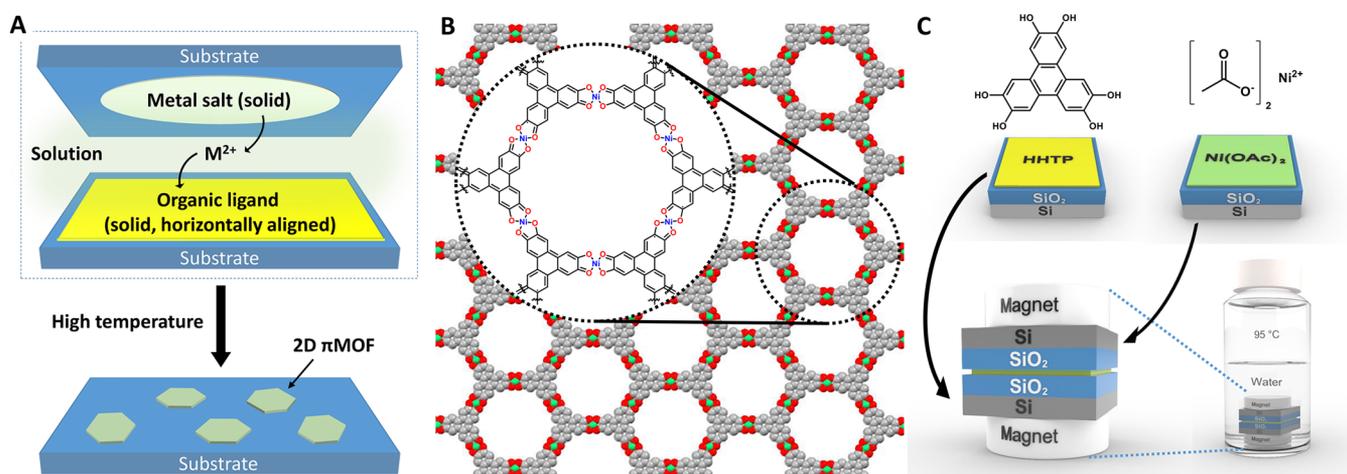
Figure 1. (A) Schematic illustration of the solution-solid growth of 2D πMOFs. The organic ligands are introduced in the solid phase and react with metal ions that are dissolved in water. The dense and aligned organic molecules increase the basal-plane growth rate. The high reaction temperature accelerates the reaction rate and ensures high crystallinity. The small volume and high aspect ratio of the reaction solution facilitate planar crystal growth. (B) MOF layer structure of Ni-CAT-1. (C) Schematic of the growth method. HHTP film is grown by vacuum thermal evaporation, and Ni(OAc)$_2$ is drop-cast on a separate substrate. The two substrates are pressed together so that the two reactants are opposite each other. Teflon-coated magnets are used to press the two substrates with a pressure of 50 kPa at room temperature. The ensemble is placed in water and heated at 95 °C. Typical growth conditions are from 40 nm-thick film of HHTP, a drop-cast film of Ni(OAc)$_2$ from 20 μL of 10 mM methanol solution, and a reaction time of 12 h.
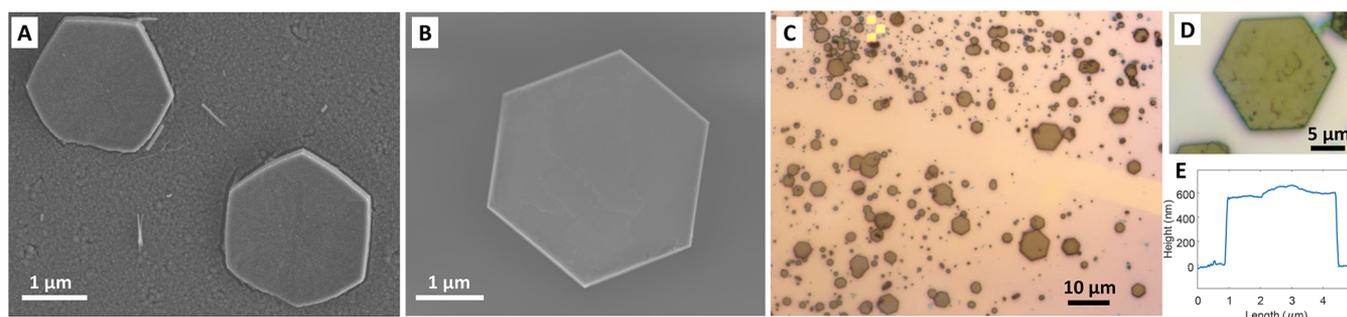

Figure 2. Single-crystal plates of Ni-CAT-1. (A) SEM image of Ni-CAT-1 crystals after a reaction time of 1 h. (B) SEM image of crystals grown after 12 h. No residual HHTP is observed surrounding the Ni-CAT-1 crystals, and the sharp edges and corners indicate increased crystallinity. (C,D) Optical microscope images of the crystal plates on a Si/SiO$_2$ substrate. (E) Thickness profile of the crystal grown from 40 nm of HHTP. The thickness can be varied by adjusting reaction conditions (Figure S8).

growth kinetics, an insufficient supply of energy to the system often leads to limited crystallinity.[24,25] Other approaches, including layer-by-layer approaches,[26] biphasic liquid−gas interfacial methods,[16] and vapor-induced growth[27] have also been limited thus far to polycrystalline films with crystallites exhibiting small basal plane domains.

In this work, we demonstrate the single-crystal growth of Ni-CAT-1. It is one of the first reported 2D πMOFs,[12] and it is based on a stable organic ligand in contrast to air-sensitive ligands adopted in more conductive 2D πMOFs.[15,20,23] Hence this material is chosen as the testbed for a new growth technique for 2D πMOFs that promotes the growth of plate-shaped rather than needle-shaped single crystals.

■ RESULTS AND DISCUSSION

The aim is to increase the rate of metal−ligand bond formation, leading to π−d conjugation, relative to the rate of layers stacking along the *c* axis. This is achieved by maintaining high concentrations of the reactants and a high temperature. We employ a biphasic solution-solid approach shown in Figure 1, wherein the organic ligand, here hexahydroxytriphenylene (HHTP), is deposited as a thin film on a silicon substrate by vacuum thermal evaporation. A planar molecular structure and strong hydrogen bonding act[28,29] to align the HTTP molecules in the plane of the silicon substrate, thereby defining the growth direction for the 2D πMOF crystals. Indeed, an ellipsometric measurement of an HHTP film deposited on silicon demonstrates horizontal alignment. HHTP has higher polarizability along the molecular plane, and the measured ordinary refractive index exceeds the extraordinary index (Figure S1). The order parameter of the film is −0.22, which is typical for small molecules that exhibit preferential horizontal alignment after vacuum thermal evaporation.[28] For reference, the measured order parameter is −0.5 if the molecules have perfect horizontal alignment and 0 if they are randomly oriented.[28] Importantly, because essentially all organic ligands used to synthesize 2D πMOFs have planar structures, thermal evaporation should afford similarly ordered and oriented films with many such ligands.

Another key aspect of our growth method is to confine the reaction volume to a very thin layer between substrates tightly held together by magnets, one in contact with a substrate for the ligand film, the other in contact with a substrate for a solid film of the metal salt precursor. The entire assembly is
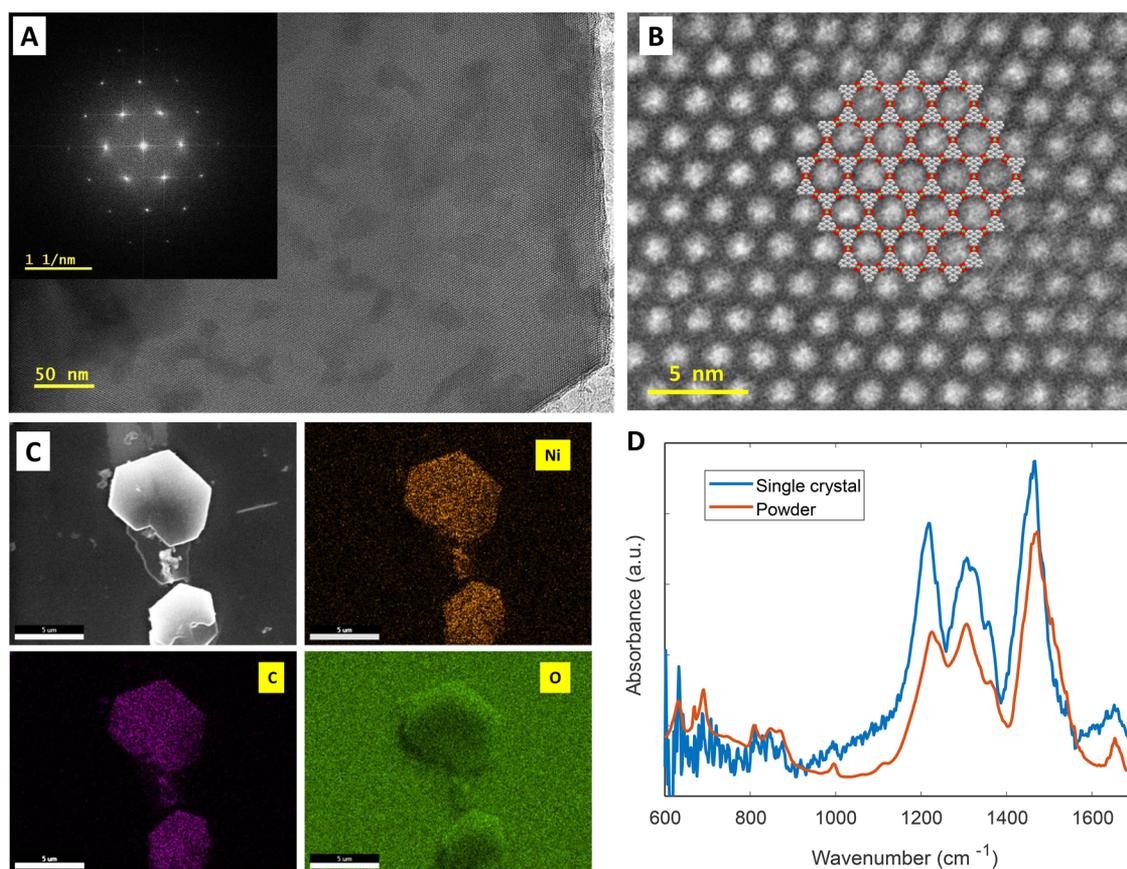
Figure 3. Characterization of the 2D πMOF crystals. (A) Low-magnification bright-field TEM image of a Ni-CAT-1 crystal. Because of the large unit cell of the MOF, the lattice is visible at this low magnification, with its expected uniform hexagonal structure. A hexagonal vertex of a single crystal is clearly visible in the bottom right corner. Inset: The corresponding Fourier transform image confirms a lattice spacing of 2.1 nm. (B) High-magnification bright-field TEM image superimposed with a generated crystal structure of Ni-CAT-1. (C) Elemental mapping of the crystals by EDS, showing a uniform distribution of nickel and carbon. The strong oxygen background signal is due to the SiO$_2$ substrate. The elemental analysis is shown in Figure S10. (D) IR spectrum of powder and single crystal Ni-CAT-1, confirming similar vibrational features. The identity of Ni-CAT-1 powder was confirmed by PXRD (Figure S9).

immersed in a solvent and heated to an appropriate temperature (Figure 1C). This configuration provides several key advantages: (1) it allows only a very small thin layer of solvent to be present during the reaction; (2) the limited solvent exposure in the thin layer maintains HHTP largely in the solid phase; and (3) the magnet assembly minimizes crystal growth in the *c* direction but allows essentially unimpeded growth in the basal plane. For our testbed material Ni-CAT-1, an oriented film of HHTP is placed in contact with a solid film dropcast from a solution of nickel acetate, Ni(OAc)$_2$. The two films, both deposited on silicon covered by a thin layer of SiO$_2$, are squeezed between two commercial neodymium coin magnets and heated in water at 95 °C (Figure 1C). The narrow space (less than 1 μL; see supplementary text) between the films of the two reactants permits small amounts of water between the metal and organic substrates. Because of the poor solubility of HHTP in water (0.2 g/L at 95 °C), the 40 nm film of HHTP remains largely solid, whereas Ni(OAc)$_2$ dissolves. Consequently, MOF nuclei can form on the HHTP film, growing rapidly in the high concentration of aligned HHTP molecules. Since MOF crystals are porous, we speculate that the metal ions can easily penetrate the HHTP layer as the reaction proceeds. We confirm the persistence of a solid film of HHTP in water when confined between two substrates in the absence of nickel acetate (Figure S2): when the HHTP film is

not covered with another substrate, it dissolves rapidly in water.

Optical microscope and scanning electron microscope (SEM) images of typical single-crystal plates of Ni-CAT-1 grown by the method described above are shown in Figure 2. The morphology of these crystals strongly contrasts with previously reported Ni-CAT-1 needle-shaped crystals. The lateral dimension of the solution-solid grown crystals is more than 2 orders of magnitude larger than the needle-shaped ones.[12,13] After allowing the reaction to proceed for 1 h, part of the HHTP film is converted to MOF crystal plates due to the solution-solid growth as shown in Figure 2A. When we varied the reaction time from 30 min to 12 h, SEM images suggested increased crystallinity with longer reaction time (Figures 2A,B, S3). This indicates the reaction is reversible, allowing multiple nuclei to merge and/or allowing for error correction during crystal growth. To test the effect of horizontal alignment of the HHTP precursor, we repeated the process with a drop-cast polycrystalline film of HHTP with random crystallite orientation. The drop-cast HHTP generates crystals with small grains, and a greater fraction of out-of-plane crystal growth is observed compared with the crystals grown from the evaporated HHTP (Figure S4). Furthermore, using a "good" solvent for HHTP, that is, a solvent that solubilizes HHTP readily such as a water-dimethylformamide (30%) mixture,
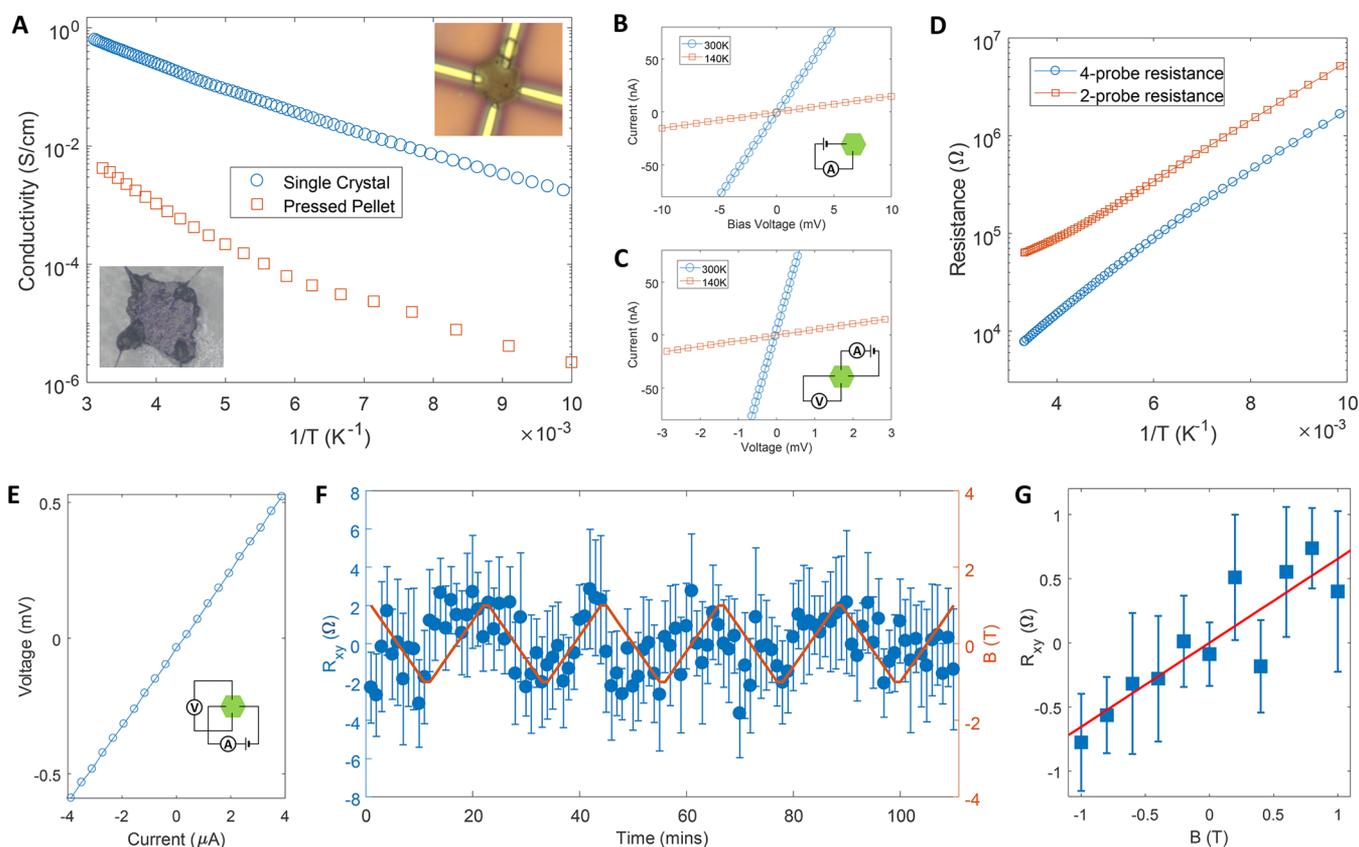
Figure 4. Electrical properties of Ni-CAT-1. (A) Temperature dependence of electrical conductivity along the basal plane of a single crystal and of a pressed pellet. Inset: optical microscope images of single-crystal and pressed-pellet devices. (B and C) Current−voltage (I−V) curves of 2-probe (B) and 4-probe (C) measurements on a single crystal. (D) Temperature dependence of 2-probe and 4-probe resistance. (E) I−V characteristics of Hall measurement at room temperature and 1 T. (F) Hall resistance (R_{xy}, blue circle) as a function of time, while the magnetic field (B, red line) is slowly swept between −1 and 1 T. The Hall resistance is determined from the slope of I−V curve in (E) and subtracting magnetic-field independent offset (Figure S14). (G) Mean Hall resistances as a function of the magnetic field. The Hall coefficient is −0.46 ± 0.14 cm³/C, indicating that the high conductivity of Ni-CAT-1 originates from a high carrier density. Error bars are the standard error of the mean.

large rod-shape crystals were generated because this solvent mixture dissolved the entire HHTP film, which is no longer oriented (Figure S5). Finally, a systematic increase of the reaction space between the magnets by increasing the diameter of dispersed microspheres from Ø 4 to 49 μm produced crystals with a morphology that varied from plate-like to needle-like (Figure S6). These series of experiments attest to the critical role of a solid, oriented film of HHTP as a precursor. Note that the solution-solid growth method also generates some rod-shape crystals and polycrystals (Figure S7). We speculate that the different morphologies are caused by variation in the local concentration of nickel acetate from the drop-casting and wetting process. Residual HHTP dissolved in water can initiate conventional single-phase solution growth that generates rod-shaped crystals.

Transmission electron microscopy (TEM), energy dispersive spectroscopy (EDS), and Fourier-transform infrared spectroscopy (FT-IR) confirmed the identity and integrity of the single-crystal plates, as shown in Figure 3. A TEM image of one corner of a crystal plate is shown in Figure 2A. The large crystal has a uniform hexagonal structure. The fast Fourier transform (FFT) of the image confirms single-crystallinity and gives a lattice parameter of 2.1 nm, which is consistent with the powder X-ray diffraction (PXRD) data (Figure S9). The EDS elemental maps demonstrate a uniform distribution of nickel and carbon with a Ni:C ratio of 1:12, in agreement with the

stoichiometry of Ni-CAT-1 (Figure S10). FTIR further confirms the identity of the crystals, with the vibrational bands of Ni-CAT-1 single crystals overlapping those observed for powder samples. The latter were independently verified as pure Ni-CAT-1 by PXRD.[12] To check the applicability of the solution-solid growth, we changed nickel acetate to cobalt acetate under identical growth conditions, and planar crystals of Co-CAT-1 were produced as shown in Figure S17 and Figure S18.

The large single crystals of Ni-CAT-1 permit measurements of the basal plane's electrical properties in 2D πMOFs. To minimize damage to the 2D πMOFs during device fabrication, we placed four electrical contacts using a stencil mask technique rather than conventional electron beam lithography. The stencil mask avoids electron beam resist coating, baking, and direct electron-beam exposure. Details of the sample fabrication techniques and conductivities are given in the Supporting Information and Figure S11. Conventional 4-probe pressed pellet samples provided important comparisons with the single crystal devices. We find that the peak basal-plane single-crystal electrical conductivity of the Ni-CAT-1 crystals is 2 S/cm, with an average of 0.8 S/cm and a standard deviation of 0.7 S/cm, whereas the conductivity of a polycrystalline pressed-pellet sample is 3.6 × 10⁻³ S/cm, similar to two previously reported values.[11,30] In other words, the conductivity of a polycrystalline pressed pellet of Ni-CAT-1 is

lower by more than 2 orders of magnitude than that of the single crystals as may be expected given the grain boundaries and contributions from the out-of-plane transport. The conductivity along the c axis is estimated at 1×10^{-4} S/cm from a two probe device (Figure S12). The presence of traps at grain boundaries is further confirmed by a temperature-dependent conductivity study (Figure 4A). The Arrhenius behavior of the temperature-dependent conductivity yields an activation energy of 0.09 eV for the single crystal, and 0.14 eV for the pressed pellet devices.

A Hall measurement on a single crystal device of Ni-CAT-1 provides unique insight into the nature of in-plane electrical transport in 2D πMOFs. The Hall coefficient obtained from fitting the data in Figure 4G, (-0.46 ± 0.14) cm^3/C, is relatively small, suggesting that the origin of the high conductivity in this particular material is a high carrier concentration rather than fast carrier transport. The thermally activated conductivity indicates Ni-CAT-1 is a semiconductor. It may intrinsically possess high densities of electrons and holes at room temperature given its small bandgap of 0.2 eV (Figure S13). However, assuming n-type behavior, consistent with the sign of the Hall coefficient, gives an electron density of $(-1.4 \pm 0.42) \times 10^{19}$ cm^{-3}, which corresponds to 1% of the HHTP-site density, and a corresponding electron mobility of (0.16 ± 0.049) cm^2/V·sec; see supplementary Table 1 for representative comparisons with other electronic materials. Whereas the single crystals of Ni-CAT-1 generate a distinct Hall effect, we were unable to measure the Hall effect in pressed pellet samples due to suppression of the charge carrier mobility by grain boundaries. Recalling that the pressed pellet samples also exhibited nearly 3 orders of magnitude decrease in conductivity, these measurements provide an important direct assessment of charge carrier densities in 2D πMOFs and confirm that the single crystal samples exhibit significantly superior electronic properties overall.

Biphasic solution-solid growth of large planar single crystals of Ni-CAT-1 allow characterization of its intrinsic electronic properties along the 2D plane. Based on these promising results, we further anticipate that application of this growth technique will enhance the performance of other, highly conductive 2D πMOFs.[15,20,23] Future study of single-crystal 2D πMOFs should clarify fundamental structure−property relationships and allow measurement of intrinsic electronic and topologically protected properties.

■ ASSOCIATED CONTENT

ⓢ Supporting Information

The Supporting Information is available free of charge at https://pubs.acs.org/doi/10.1021/acscentsci.0c01488.

> Materials and Methods, Supplementary Text, Figures S1 to S20, Tables S1 and S2 (PDF)

■ AUTHOR INFORMATION

Corresponding Authors

Mircea Dincă − *Department of Chemistry, Massachusetts Institute of Technology, Cambridge, Massachusetts 02139, United States;* ⓞ orcid.org/0000-0002-1262-1264; Email: mdinca@mit.edu

Marc A. Baldo − *Department of Electrical Engineering and Computer Science, Massachusetts Institute of Technology, Cambridge, Massachusetts 02139, United States;* ⓞ orcid.org/0000-0003-2201-5257; Email: baldo@mit.edu

Authors

Dong-Gwang Ha − *Department of Materials Science and Engineering, Massachusetts Institute of Technology, Cambridge, Massachusetts 02139, United States*

Mehdi Rezaee − *School of Engineering and Applied Sciences, Harvard University, Cambridge, Massachusetts 02138, United States*

Yimo Han − *Department of Applied and Engineering Physics, Cornell University, Ithaca, New York 14853, United States;* ⓞ orcid.org/0000-0003-0563-4611

Saima A. Siddiqui − *Department of Electrical Engineering and Computer Science, Massachusetts Institute of Technology, Cambridge, Massachusetts 02139, United States*

Robert W. Day − *Department of Chemistry, Massachusetts Institute of Technology, Cambridge, Massachusetts 02139, United States*

Lilia S. Xie − *Department of Chemistry, Massachusetts Institute of Technology, Cambridge, Massachusetts 02139, United States*

Brian J. Modtland − *Department of Electrical Engineering and Computer Science, Massachusetts Institute of Technology, Cambridge, Massachusetts 02139, United States*

David A. Muller − *Department of Applied and Engineering Physics, Cornell University, Ithaca, New York 14853, United States; Kavli Institute at Cornell for Nanoscale Science, Ithaca, New York 14853, United States*

Jing Kong − *Department of Electrical Engineering and Computer Science, Massachusetts Institute of Technology, Cambridge, Massachusetts 02139, United States;* ⓞ orcid.org/0000-0003-0551-1208

Philip Kim − *School of Engineering and Applied Sciences and Department of Physics, Harvard University, Cambridge, Massachusetts 02138, United States*

Complete contact information is available at:
https://pubs.acs.org/10.1021/acscentsci.0c01488

Author Contributions

D.-G.H. and M.A.B. conceived the project. D.-G.H. developed the growth method and characterized the material. D.-G.H., M.R., and S.A.S. made single-crystal devices. D.-G.H. and L.S.X. made and characterized pressed-pellet devices. D.-G.H. and M.R. measured electrical properties. D.-G.H. and Y.H. measured TEM. R.W.D. made and characterized devices for the out-of-plane conductivity. B.J.M. contributed to analysis. D.A.M. supervised TEM measurement. P.K. supervised electrical characterization. J.K., M.D., and M.A.B. supervised the growth and characterization of the material. All authors discussed the results and commented on the manuscript.

Notes

The authors declare no competing financial interest.

■ ACKNOWLEDGMENTS

Perkinson for help with the ellipsometry and polarizing microscopy measurements.

■ REFERENCES

(1) Yaghi, O.; O'Keeffe, M.; Ockwig, N.; Chae, H.; Eddaoudi, M.; Kim, J. Reticular synthesis and the design of new materials. *Nature* **2003**, *423*, 705.

(2) Ferey, G. Hybrid porous solids: past, present, future. *Chem. Soc. Rev.* **2008**, *37*, 191−214.

(3) Batten, S. R.; Champness, N. R.; Chen, X.; Garcia-martinez, J.; Kitagawa, S.; Öhrström, L.; O'Keeffe, M.; Paik Suh, M.; Reedijk, J. Terminology of metal − organic frameworks and coordination polymers (IUPAC Recommendations 2013)*. *Pure Appl. Chem.* **2013**, *85*, 1715−1724.

(4) Sheberla, D.; Bachman, J. C.; Elias, J. S.; Sun, C.; Shao-horn, Y.; Dincǎ, M. Conductive MOF electrodes for stable supercapacitors with high areal capacitance. *Nat. Mater.* **2017**, *16*, 220.

(5) Feng, D.; Lei, T.; Lukatskaya, M. R.; Park, J.; Huang, Z.; Lee, M.; Shaw, L.; Chen, S.; Yakovenko, A. A.; Kulkarni, A.; Xiao, J.; Fredrickson, K.; Tok, J. B.; Zou, X.; Cui, Y.; Bao, Z. Robust and conductive two-dimensional metal−organic frameworks with exceptionally high volumetric and areal capacitance. *Nat. Energy* **2018**, *3*, 30.

(6) Gao, G.; Zheng, F.; Pan, F.; Wang, L. W. Theoretical Investigation of 2D Conductive Microporous Coordination Polymers as Li−S Battery Cathode with Ultrahigh Energy Density. *Adv. Energy Mater.* **2018**, *8*, 1801823.

(7) Wu, M.; Wang, Z.; Liu, J.; Li, W.; Fu, H.; Sun, L.; Liu, X.; Pan, M.; Weng, Hongming; Dincǎ, M.; Fu, L.; Li, J. Conetronics in 2D metal-organic frameworks: double/half Dirac cones and quantum anomalous Hall effect. *2D Mater.* **2017**, *4*, 015015.

(8) Zhao, B.; Zhang, J.; Feng, W.; Yao, Y.; Yang, Z. Quantum spin Hall and Z_2 metallic states in an organic material. *Phys. Rev. B: Condens. Matter Mater. Phys.* **2014**, *90*, 201403.

(9) Wang, Z. F.; Su, N.; Liu, F. Prediction of a Two-Dimensional Organic Topological Insulator. *Nano Lett.* **2013**, *13*, 2842−2845.

(10) Sun, L.; Campbell, M. G.; Dincǎ, M. Electrically Conductive Porous Metal−Organic Frameworks. *Angew. Chem., Int. Ed.* **2016**, *55*, 3566−3579.

(11) Ko, M.; Mendecki, L.; Mirica, K. A. Conductive two-dimensional metal-organic frameworks as multifunctional materials. *Chem. Commun.* **2018**, *54*, 7873−7891.

(12) Hmadeh, M.; Lu, Z.; Liu, Z.; Gándara, F.; Furukawa, H.; Wan, S.; Augustyn, V.; Chang, R.; Liao, L.; Zhou, F.; Perre, E.; Ozolins, V.; Suenaga, K.; Duan, X.; Dunn, B.; Yamamto, Y.; Terasaki, O.; Yaghi, O. M. New Porous Crystals of Extended Metal-Catecholates. *Chem. Mater.* **2012**, *24*, 3511−3513.

(13) Smith, M. K.; Jensen, K. E.; Pivak, P. A.; Mirica, K. A. Direct Self-Assembly of Conductive Nanorods of Metal-Organic Frameworks into Chemiresistive Devices on Shrinkable Polymer Films. *Chem. Mater.* **2016**, *28*, 5264.

(14) Dou, J.; Sun, L.; Ge, Y.; Li, W.; Hendon, C. H.; Li, J.; Gul, S.; Yano, J.; Stach, E. A.; Dinca, M. Signature of Metallic Behavior in the Metal − Organic Frameworks. *J. Am. Chem. Soc.* **2017**, *139*, 13608.

(15) Sheberla, D.; Sun, L.; Blood-Forsythe, M. A.; Er, S.; Wade, C. R.; Brozek, C. K.; Aspuru-Guzik, A.; Dincǎ, M. High Electrical Conductivity in Ni3(2,3,6,7,10,11-hexaiminotriphenylene)2, a Semiconducting Metal−Organic Graphene Analogue. *J. Am. Chem. Soc.* **2014**, *136*, 8859−8862.

(16) Rubio-Giménez, V.; Galbiati, M.; Castells-Gil, J.; Almora-Barrios, N.; Navarro-Sánchez, J.; Escorcia-Ariza, G.; Mattera, M.; Arnold, T.; Rawle, J.; Tatay, S.; Coronado, E.; Martí-Gastaldo, C. Bottom-Up Fabrication of Semiconductive Metal−Organic Framework Ultrathin Films. *Adv. Mater.* **2018**, *30*, 1704291.

(17) Huang, X.; Sheng, P.; Tu, Z.; Zhang, F.; Wang, J.; Geng, H.; Zou, Y.; Di, C.-a.; Yi, Y.; Sun, Y.; Xu, W.; Zhu, D. A two-dimensional p−d conjugated coordination polymer with extremely high electrical conductivity and ambipolar transport behaviour. *Nat. Commun.* **2015**, *6*, 7408.

(18) Clough, A. J.; Skelton, J. M.; Downes, C. A.; de la Rosa, A. A.; Yoo, J. W.; Walsh, A.; Melot, B. C.; Marinescu, S. C. Metallic Conductivity in a Two-Dimensional Cobalt Dithiolene Metal − Organic Framework. *J. Am. Chem. Soc.* **2017**, *139*, 10863.

(19) Dong, R.; Han, P.; Arora, H.; Ballabio, M.; Karakus, M.; Zhang, Z.; Shekhar, C.; Adler, P.; Petkov, P. S.; Erbe, A.; Mannsfeld, S. C. B.; Felser, C.; Heine, T.; Bonn, M.; Feng, X.; Cánovas, E. High-mobility band-like charge transport in a semiconducting two-dimensional metal−organic framework. *Nat. Mater.* **2018**, *17*, 1027−1032.

(20) Kambe, T.; Sakamoto, R.; Hoshiko, K.; Takada, K.; Miyachi, M.; Ryu, J.-H.; Sasaki, S.; Kim, J.; Nakazato, K.; Takata, M.; Nishihara, H. π-Conjugated Nickel Bis(dithiolene) Complex Nanosheet. *J. Am. Chem. Soc.* **2013**, *135*, 2462−2465.

(21) Kambe, T.; Sakamoto, R.; Kusamoto, T.; Pal, T.; Fukui, N.; Hoshiko, K.; Shimojima, T.; Wang, Z.; Hirahara, T.; Ishizaka, K.; Hasegawa, S.; Liu, F.; Nishihara, H. Redox Control and High Conductivity of Nickel Bis(dithiolene) Complex π-Nanosheet: A Potential Organic Two-Dimensional Topological Insulator. *J. Am. Chem. Soc.* **2014**, *136*, 14357−14360.

(22) Pal, T.; Kambe, T.; Kusamoto, T.; Foo, M. L.; Matsuoka, R.; Sakamoto, R.; Nishihara, H. Interfacial Synthesis of Electrically Conducting Palladium Bis(dithiolene) Complex Nanosheet. *ChemPlusChem* **2015**, *80*, 1255−1258.

(23) Huang, X.; Zhang, S.; Liu, L.; Yu, L.; Chen, G.; Xu, W.; Zhu, D. Superconductivity in a Copper(II)-Based Coordination Polymer with Perfect Kagome Structure. *Angew. Chem., Int. Ed.* **2018**, *57*, 146−150.

(24) Cheetham, A. K.; Kieslich, G.; Yeung, H. H. M. Thermodynamic and Kinetic Effects in the Crystallization of Metal-Organic Frameworks. *Acc. Chem. Res.* **2018**, *51*, 659−667.

(25) Stock, N.; Biswas, S. Synthesis of Metal-Organic Frameworks (MOFs): Routes to Various MOF Topologies, Morphologies, and Composites. *Chem. Rev.* **2012**, *112*, 933−969.

(26) Yao, M. S.; Lv, X. J.; Fu, Z. H.; Li, W. H.; Deng, W. H.; Wu, G. D.; Xu, G. Layer-by-Layer Assembled Conductive Metal−Organic Framework Nanofilms for Room-Temperature Chemiresistive Sensing. *Angew. Chem., Int. Ed.* **2017**, *56*, 16510−16514.

(27) Yuan, K.; Song, T.; Zhu, X.; Li, B.; Han, B.; Zheng, L.; Li, J.; Zhang, X.; Hu, W. Construction of Large-Area Ultrathin Conductive Metal − Organic Framework Films through Vapor-Induced Conversion. *Small* **2019**, *15*, 1804845.

(28) Yokoyama, D. Molecular orientation in small-molecule organic light-emitting diodes. *J. Mater. Chem.* **2011**, *21*, 19187.

(29) Kim, H. J.; Lee, J. H.; Kim, J. W.; Lee, S.; Jang, J.; Lee, H. H.; Kim, J. J. Molecular alignment and nanostructure of 1,4,5,8,9,11-hexaazatriphenylene- hexanitrile (HATCN) thin films on organic surfaces. *J. Mater. Chem. C* **2013**, *1*, 1260−1264.

(30) Miner, E. M.; Wang, L.; Dincǎ, M. Modular O_2 electro-reduction activity in triphenylene-based metal−organic frameworks. *Chem. Sci.* **2018**, *9*, 6286−6291.